0 0 0 0 4 7 0 0 5 7 8

Submitted to Metallurgical Transactions
(In Press)

UC-25

LBL-6067
Preprint

RECEIVED
LAWRENCE
BERKELEY LABORATORY

MAR 8 1978

LIBRARY AND
DOCUMENTS SECTION

LATTICE IMAGING AND OPTICAL MICRO-ANALYSIS OF A Cu-Ni-Cr SPINODAL ALLOY

C. K. Wu, R. Sinclair, and
G. Thomas

October 1977

Prepared for the U. S. Department of Energy
under Contract W-7405-ENG-48

For Reference

Not to be taken from this room

LAWRENCE BERKELEY LABORATORY
UNIVERSITY OF CALIFORNIA
BERKELEY

LBL-6067

DISCLAIMER

This document was prepared as an account of work sponsored by the United States Government. While this document is believed to contain correct information, neither the United States Government nor any agency thereof, nor the Regents of the University of California, nor any of their employees, makes any warranty, express or implied, or assumes any legal responsibility for the accuracy, completeness, or usefulness of any information, apparatus, product, or process disclosed, or represents that its use would not infringe privately owned rights. Reference herein to any specific commercial product, process, or service by its trade name, trademark, manufacturer, or otherwise, does not necessarily constitute or imply its endorsement, recommendation, or favoring by the United States Government or any agency thereof, or the Regents of the University of California. The views and opinions of authors expressed herein do not necessarily state or reflect those of the United States Government or any agency thereof or the Regents of the University of California.

0 0 0 0 4 7 0 8 5 7 9

LBL-6067

LATTICE IMAGING AND OPTICAL MICRO-ANALYSIS OF A Cu-Ni-Cr SPINODAL ALLOY

C. K. Wu, R. Sinclair*, and G. Thomas

Materials and Molecular Research Division, Lawrence Berkeley Laboratory and Department of Materials Science and Mineral Engineering, University of California, Berkeley, CA 94720

* Department of Materials Science and Engineering, Stanford University, Stanford, CA 94305

0 0 0 0 4 7 0 8 5 8 0

ABSTRACT

The lattice imaging technique of high-resolution electron microscopy has been applied to study spinodal decomposition in a Cu-Ni-Cr alloy. The reliability of various methods for processing the image data is discussed. The important parameters describing a spinodal microstructure (viz., composition amplitude, wavelength of modulations, and relative volume fractions of the two phases) can all be obtained from the lattice image, even though the maximum change of lattice parameters between the two phases is only ~1%. Interesting interfacial microstructural features have also been revealed from micro-optical diffractograms of the images during later stages of aging.

1. Introduction

A spinodally decomposed product may be characterized by small composition fluctuations over large distances. Studies by x-ray diffraction (e.g. 1) reveal only the wavelength of the early stage modulation and the average modulation amplitude through diffracted intensities, which are averaged over a large specimen volume. Conventional bright-field or dark-field images obtained by transmission electron microscopy (TEM) cannot provide any compositional information about the two phases (e.g. 2,3). It is only possible to detect the localized, plane-by-plane variations in composition directly by corresponding lattice parameter modulations through the lattice imaging technique (4,5).

Gronsky et al. (4,5) first used lattice imaging for studying spinodal alloys. In preliminary results of spinodally decomposed Au-77 at .% Ni, lattice parameter differences (Δa) were clearly detected from one region to another by measurements on microdensitometer traces across the lattice fringes. In addition, the average wavelength determined from this technique was in exact agreement with that determined from the positions of satellite reflections in the corresponding diffraction patterns. Thus, the lattice image of this material reveals the principal features expected of a spinodally decomposed alloy, and laser optical diffraction from the lattice image negatives also showed characteristic satellite reflections. This latter method allows areas as small as 10Å (1 nm) in diameter to be chosen to give diffraction data which are far superior in terms of resolution to those from selected area electron diffraction (5). These optical diffraction patterns can also be used to obtain

fringe spacing changes (6,7) and are an alternative to the microdensitometer measurements for obtaining fringe spacing information.

For the present research, Cu-Ni-Cr was studied particularly because of its commercial importance as an alloy with good strength and corrosion resistance in marine environments (8). From conventional TEM studies of this alloy (9) it is known that the material spinodally decomposes into Cu-rich and Cu-poor regions when aged at temperatures below 760°C (1033 K), and the difference in lattice parameters between the two phases is quite small (10) ($\Delta a \sim 1\%$). Hence the analysis of the fringe spacings must be performed very carefully in order to achieve meaningful results from the lattice images. Three different methods were used to determine Δa from fringe spacings. As decomposition occurs along the so-called elastically "soft" ⟨100⟩ directions (9), the (200) lattice fringes were imaged to measure Δa.

2. Experimental Procedures

2.1 The Material and Heat-Treatment

The alloy was kindly provided by International Nickel Company. Chemical analysis done at the Paul D. Merica Laboratory gave the following results, expressed in weight %:

Ni-28.9%	Ti-0.051%
Cr-2.84%	Si-0.091%
Mn-0.55%	Fe-0.32%
Zr-0.22%	Cu-balance
C-0.014%	

The alloy was first encapsulated in evacuated quartz tubes, homogenized at 1100°C for 72 hours, quenched into ice brine and cold rolled to 10 mils (254 μm) thickness for transmission electron microscope specimens.

After cutting and machining, the various experimental specimens were re-annealed in quartz tubes filled with purified argon at 1100°C for two hours and quenched again in ice brine.

Specimens were subsequently aged at 600°C and 700°C for various times from 5 min. to 808 hours.

2.2 Polishing Procedures

The heat-treated alloys were chemically polished in a solution of 3 parts HNO_3 and 1 part HF at room temperature to a thickness of 3-5 mils, and then mechanically polished on (600) grit emery paper. Small discs were punched from the alloys and thin foils for TEM were prepared by jet-electropolishing, using the following conditions:

solution: 125 ml nitric acid and 375 ml methanol

temperature: -20°C to -25°C (cold methanol was used as a cooling bath)

polishing voltage: 20V (DC)

2.3 Lattice Imaging

For lattice imaging, a Philips EM 301 transmission electron microscope equipped with a high-resolution stage was used. Specimen grains were found with [001] approximately parallel to the microscope optical axis. The crystal was then tilted, or translated into an area where (200) two-beam conditions were operable, in order to image the (200) lattice fringes.

2.4 Calibration of the Magnification

Usually, lattice imaging pictures were taken with the microscope operating at high magnification. A nominal magnification setting of 570,000x was employed but the true magnification generally varies from this value, so it is necessary to calibrate the magnification for obtaining accurate measurements of absolute fringe spacings. This was done by finding the average lattice constant of the alloy at each aging condition by standard x-ray diffraction methods and equating this value to the average corresponding (200) fringe spacing on the micrograph.

2.5 Measurement of Fringe Spacings

The three different methods used to measure the variations of fringe spacings between the two phases from lattice image negatives are as follows:

(a) Optical diffraction: The lattice image negatives were placed in the path of a He-Ne laser beam in a standard optical bench. The fringes present on the negatives give rise to diffraction spots in the back focal plane of the optical objective lens which were recorded photographically. By measuring the distance r between the transmitted and diffracted spots, and by comparison with that of standard gold (200) fringes, the corresponding d-spacing can thus be determined.

(b) Microdensitometer trace analysis: The individual fringe spacings can be found by directly measuring the distance from peak to peak on a microdensitometer plot of the image and dividing by the appropriate magnification. In this research, average values were obtained over 15 fringe spacings at a time, and standard deviations

were calculated to give the accuracy limits. The final shape of the fringe spacing-distance curve then shows the variations of the fringe spacings and lattice parameter.

(c) Direct measurement from enlarged micrographs: It is straightforward to measure the fringe spacings on an enlarged micrograph, divide by the magnification and obtain the actual fringe spacings.

2.6 Accuracy of Measurement

A general assessment of the accuracy of these methods has been made elsewhere (11). Since in the present alloy the lattice fringes were often of low visibility, the most convenient and reliable method of analysis was by optical diffraction, although this is not usually the case.

(a) The main limitation of the optical diffraction technique is given by the aperture size, since the aperture governs the breadth of the diffraction spot and will itself diffract. Figure 1 shows optical diffraction patterns centered on the same area in the negative using three different aperture sizes. When the aperture size is less than 35 Å, Fraunhofer scattering from the aperture may interfere with the diffracted spots (e.g. Fig. 1a). It is also more difficult to locate the exact center of the diffraction spots as they are broadened and hence the error in measurement is increased. By sacrificing resolution and averaging over a larger number of fringes, larger apertures give sharper diffraction spots (Figures 1b,c) resulting in more accurate measurements. Generally, using a rule marked down to 0.5mm, the uncertainty in measuring the distance between the diffracted spots is ~0.5%.

(b) Microdensitometer trace analysis will provide more accurate data as long as there are easily recognizable and high contrast fringes in the negative. Figure 2 shows lattice fringes of a pure gold specimen and the corresponding microdensitometer trace. Since the fringes are clear in the micrograph, the microdensitometer trace is also very sharp and the fringe positions can be easily identified from the peaks in the plot. In Cu-Ni-Cr, however, the exact position of each peak sometimes becomes unidentifiable because the image contrast in the alloy is not as strong as in pure metals. Also, dark and bright diffraction contrast occurs due to the decomposition and this masks the exact position of some fringes. This effect is illustrated in Figure 3. The fringe positions are smeared and broadened and thus the accuracy is considerably reduced over what is more generally attained.

In order to reduce these experimental errors, average values may be taken over several fringes. In this research, by averaging over 15 fringe spacings at a time, the accuracy was estimated to be ~1.0%.

(c) The prints from these images provide a less objective criterion for assessing the fringe spacings than do the microdensitometer traces. Again, the accuracy can be improved if measurements are averaged over a number of fringes and is estimated here to be ~2% for 10 fringes.

3. Results

For a perfect crystal, the electron image fringe spacings are identical to the lattice spacings in specimens at the exact Bragg imaging condition (12). In a crystal with variable d-spacings (as in a spinodal product), the situation is more complex, and the fringe

spacings may not directly relate to the actual interplanar spacings in the alloy (13). However, the measured fringe spacings in the later stages of decomposition in this research have been correlated with previous x-ray data from the two-phase material (10). The results indicate that the fringe and lattice spacings are identical within experimental error, so that it is reasonable to assume that the lattice imaging method can be applied to the earlier stages of aging as well, in order to obtain lattice parameter differences.

By measuring fringe spacings, the localized lattice parameter of the specimen can be obtained. Since the lattice constants depend on composition, then the lattice imaging method is useful for estimating compositions in the crystal. Thus composition profiles in the material can be shown at resolutions down to the atomic plane level by plotting fringe spacing variations versus distance.

3.1 Early Stages of Decomposition

At the early stages of spinodal decompostion, solute segregation occurs to produce a wavelike composition variation (14). The lattice is continuous throughout the crystal. A lattice image and its corresponding diffraction pattern are shown in Figure 4 for a specimen aged 10 min. at 700°C. The large-scale dark and bright contrast is typical of a modulated microstructure imaged under two-beam conditions.

The fringes are continuous from one phase to the other. Analysis of the microdensitometer trace, as described above, shows that the spacings vary periodically in the image, and produce a wavelike profile which is shown in Figure 5. The maximum and minimum lattice parameters

can be seen to be approximately 3.60 ± 0.02Å and 3.55 ± 0.02Å respectively, which is consistent with previously reported values (10) for the Cu-rich (3.603 ± 0.001 Å) and Cu-poor (3.571 ± 0.002 Å) phases and with values determined in this study. Although the uncertainties are too large to distinguish the d-spacing of adjacent fringes, the overall profile is clearly seen. In addition, the average modulation wavelength determined from this plot (48 ± 8 Å) is in good agreement with that found from the satellite spacings in the electron diffraction pattern(50 ± 5 Å) and close to measurements on the bright field micrographs (65 ± 5 Å). Whether this profile truly represents the initial wavelike composition modulation that is expected is discussed later.

Lattice images of other specimens in the early stages of aging similarly showed spacing variations from one place to another when analyzed by trace analysis or optical diffraction, with good agreement between wavelengths determined from the various methods. A compilation of approximate maximum and minimum spacings is given in Table I.

3.2 Later Stages of Decomposition

The fine, wavy microstructure of the early stages changes upon aging, such that Cu-rich and Cu-poor regions separate into two distinct phases (e.g. Figure 6). The interfaces appear to sharpen and the wavelength of the modulation increases (9). The statistical reliability of the fringe spacing analysis increases since averages may be taken over a greater number of fringes (11).

It is possible at these later stages to correlate directly the fringe spacings with the image contrast of the dispersion. In the present case, the Cu-poor phase is the minor phase and is thus isolated

into discrete particles surrounded by the Cu-rich matrix. As the Cu atom is larger, the particles should then have the smaller lattice parameter, and this is exactly what is found by the lattice image analysis.

Figures 7 and 8 show an example for an aging treatment of 808 hours at 600°C. In fig. 7a, three precipitates can be identified in the low magnification image. The rectangular area marked is enlarged in fig. 7b to show the fringes. A series of optical diffractograms taken with 120 Å equivalent diameter aperture produced the spacing profile shown in Figure 8. Thus the precipitates at positions A-B and H-J clearly have smaller lattice spacing than the matrix regions. The smaller precipitate is shared between than the matrix regions. The smaller precipitate is shared between positions E and F and apparently the matrix contribution to the average spacing is dominant in this case. This correlation between fringe spacings and image contrast was confirmed many times in this investigation, e.g. Figure 10 in which other features are also found (see Sec. 3.3). The lattice constants so determined (Table I) are within experimental error of those established by x-ray diffraction. This is an extremely important result showing that lattice fringe spacing over small regions can correspond satisfactorily to bulk data and that small lattice parameter differences can be studied by the lattice imaging technique.

3.3 Interface Composition Profiles

It is well known that the initially diffuse interface in spinodal products sharpens upon aging (14) as shown schematically in Figure 9. This is demonstrated in the present study by the differences between Figures 5 and 8. However, in the later stages of the reaction unexpected interfacial profiles were discovered which are now described.

In overaged alloys (e.g., 166 hours at 700°C), such that the interface is partially coherent (9), placing an optical diffraction aperture over the Cu-rich or Cu-poor regions clearly produces diffraction spots whose positions correspond to each phase in turn (e.g. fig. 10 a,b). With the aperture over the interface two diffraction spots are produced (Figure 10c) indicating both that the interface is sharp and that the crystal lattice is no longer continuous.

This observation was repeated for the material aged for 808 hours at 600°C, but in this case two other types of profile were also found. Firstly, near some precipitates the optically diffracted spot broadened at the interface, indicating a diffuse boundary to be present on the scale of the aperture size (120Å) (e.g., Figure 10d). Secondly, at other interfaces a satellite spot effect is produced (Fig. 10e). Close examination of the area near the interface, by a series of optical diffractograms and from the microdensitometer analysis, shows that anomalous lattice expansion occurs in the smaller spacing Cu-poor precipitate phase, and conversely anomalous lattice contraction occurs in the Cu-rich matrix phase, away from the interface itself. This superimposes an additional fine scale lattice spacing modulation on the precipitate dispersion resulting in the observed satellite phenomenon. This latter effect is quite unexpected.

Thus three types of interface can appear in the same alloy:

i) with a sharp, discontinuous composition profile (as in fig. 10c);

ii) with a diffuse, continuous composition profile (as in fig. 10d);

iii) with a fine wavelength spacing modulation, superimposed on the normal profile (as in fig. 10e).

All of these can be modified as they appear in the lattice image because of elastic strains associated with the interface misfit. Since the misfit is small in this case, the strains are also expected to be small. Nevertheless, coherency strains will affect the interface fringe-spacing profile, and hence the deduced composition profile.

4. Discussion

It is clear from the above results that lattice imaging can indeed be used for studying lattice spacing variations which may only be very small (e.g., ~1%). In the present investigation the correlation between fringe spacing with the known lattice constants of particular phases has been demonstrated (Section 3.2). However, one of the most important aspects of studying spinodal decomposition is to obtain the shape and amplitude of the composition profile. It would be tempting to take the data in Figure 5 to indicate an approximately sinusoidal waveform at the early stages of decomposition, as schematically represented in Figure 9a. Similarly Figure 8 would represent an approximately square wave, characteristic of the later stages of the reaction, as in Figure 9b. Unfortunately in this alloy the situation is not so clear-cut as the following discussion shows.

In order to obtain sufficient precision to distinguish the fringe spacings to better than 1%, it has been necessary to average over 15 fringes. The effect of such a procedure is to "smooth" the profile, whether it be ragged or whether it be sharply discontinuous.

Figure 11 shows what happens to a square-wave modulation with periodicity of 26 fringes when each point is averaged over 15 fringes (this is very similar to the experimental situation in Figure 5): a waveform is produced which is almost continuously varying in amplitude. The introduction of statistical error would make it very similar to the experimental plot of Figure 5. In addition small wavelength regions are smoothed so that they become low amplitude ripples similar to those that appear in Figure 5. The conclusion must be that our experimental results could have arisen from a square-wave modulation, quite unlike what is expected from an early stage spinodal. Whilst this is unlikely, the point cannot be ignored.

This situation has arisen because resolution has to be sacrificed in order to attain the necessary precision. Averaging with a smaller number of fringes (equivalent to about one quarter of the compositional wavelength) would show enough characteristics of the curve to establish whether it were continuously varying or not. It is apparent that this is possible for fine-scale modulations only with systems with a reasonable variation of lattice spacing with composition (e.g., $\gtrsim$5% difference in parameter between the equilibrium phases). This is the situation for Au-Ni (4,5). For alloys with smaller lattice parameter differences, as the present case, only the later stages can be studied with any certainty. As the lattice parameter differences increase, so do the coherency strains and these could further complicate the interpretation of fringe profiles at interfaces.

One of the most interesting discoveries about the reaction comes from the latter aging period, when three types of precipitate-matrix interface can be present in the same specimen as a result of coarsening.

It would be expected that two of these would coexist for some period: the sharp and the diffuse interfaces. However, the third type is somewhat unexpected; a short wavelength modulation superimposed on the normal composition profile. This configuration should be unstable. Its origin is certainly not evident from the normal solutions to Cahn's diffusion equation (15), but very recently such an effect is predicted to occur during coarsening of a spinodal microstructure (as we have here) by taking into account higher harmonic terms (16).

5. Summary and Conclusions

1. The present lattice image and optical diffraction study of spinodally decomposed Cu-Ni-Cr alloy shows the ability to detect lattice parameter differences between two finely dispersed phases even when the difference is only ~1%. This is important in the assessment of the capability of lattice imaging for phase transformation investigations.

2. Fringe spacing analysis shows excellent correlation with the bulk lattice parameters of the precipitating phases. Thus the Cu-rich regions have a lattice-constant 3.60 ± 0.02Å, and the Cu-poor regions a lattice constant 3.56 ± 0.02 Å, consistent with previous X-ray studies.

3. Three types of interface are found to occur in the same specimen by the lattice imaging and optical diffraction techniques. These are

i) sharp, discontinuous interfaces;

ii) diffuse, continuous interfaces;

iii) continuous interfaces with short wavelength spacing modulations in the vicinity of the interface.

This latter observation is quite unexpected and deserves further investigation, both experimental and theoretical.

Acknowledgements

Financial support for this work, provided from the National Science Foundation (Grant #DMR72-03269 A01) and the U. S. Energy Research and Development Administration through the Materials and Molecular Research Division, Lawrence Berkeley Laboratory, is gratefully acknowledged. The authors would also like to thank Professor R. M. Glaeser for the use of the optical diffractometer and Dr. R. Gronsky for helpful discussions. This research was done in partial fulfillment of the M. S. requirements at the University of California, Berkeley, by one of the authors (C. K. Wu).

References

1. D. de Fontaine, Ultrafine-Grain Metals, J.J. Burke and V. Weiss (eds.), p. 93. Syracuse University Press, N.Y., (1970).

2. E.P. Butler and G. Thomas, Acta Met., (1970). Vol. 18, p. 347.

3. M. Bouchard and G. Thomas, Acta Met., (1975), Vol. 23, p. 1485.

4. R. Gronsky, M. Okada, R. Sinclair and G. Thomas, 33rd Ann. Proc. of Electron Microscopy Society of America, G.W. Bailey (ed.), Claitor's Publishing Division, Baton Rouge, La., (1975), p. 22.

5. R. Sinclair, R. Gronsky and G. Thomas, Acta Met., (1976), Vol. 24, p. 789.

6. G. Thomas, R. Sinclair and R. Gronsky, Sixth European Congress on Electron Microscopy, Jerusalem, 1976, p. 114.

7. R. Gronsky, R. Sinclair, and G. Thomas, 34th Ann. Proc. of Electron Microscopy Society of America, G.W. Bailey (ed.), Claitor's Publishing Division, Baton Rouge, La. (1976), p. 494.

8. Reports on "Cu-Ni-Alloy IN-732" from International Nickel Company, Inc., (1969).

9. C.K. Wu and G. Thomas, Met. Trans, in press.

10. J.L. Meijering, G.W. Rathenau, M.G. van der Stelg, and P.B. Braun, J. Inst. Metals, 1955-1956, Vol. 84, p. 118.

11. R. Sinclair and G. Thomas, Met Trans., in press.

12. P.B. Hirsch, A. Howie, R.B. Nicholson, D.W. Pashley, and M.J. Whelan, "Electron Microscopy of Thin Crystals," (1965), London, Butterworths, p. 160.

13. D.J.H. Cockayne, 34th Ann. Proc. of Electron Microscopy Society of America, G.W. Bailey (ed.), Claitor's Publishing Division, Baton Rouge, La., (1976), p.2.

14. J.E. Hilliard, "Phase Transformations" ASM (1970), p. 497.

15. J.W. Cahn, Acta Met., (1961), Vol. 9, p. 795.

16. A.G. Khachaturyan and J.W. Morris, Jr., Dept. of Materials Sci. and Engr., Univ. of Ca., Berkeley, private communication, Feb. 1977.

FIGURE CAPTIONS

Fig. 1. Optical diffraction patterns taken from the same area with different equivalent aperture sizes: (a)~35Å (b)~55Å (c)~120Å.

Fig. 2. Lattice image and microdensitometer traces of Au (200) fringes, showing clear distinct peaks.

Fig. 3. Lattice image and microdensitometer traces of Cu-Ni-Cr (200) fringes after aging at 600°C for 1 hour. The peaks have much lower visibility than those in Fig. 2.

Fig. 4. (200) lattice imaging micrograph of alloy aged at 700°C for 10 min. and its corresponding diffraction pattern. d_1 is the fringe spacing of the Cu-rich (bright) region while d_2 is that of the Cu-poor (dark) region.

Fig. 5. Microdensitometer trace analysis of Fig. 4. Fringe spacings change in a periodic manner and λ calculated from this plot is ~48 ± 8Å. Error bars represent standard deviations.

Fig. 6. Bright-field TEM micrograph of specimen aged 500 hours at 600°C. The particles are readily distinguished and the interface has sharpened considerably.

Fig. 7. (a) Low magnification lattice imaging micrograph shows three precipitates in the matrix. (b) Enlarged micrograph of the rectangular area marked in a. (200) lattice fringes can be resolved. Letters A-K indicate the places where an optical aperture is placed to obtain the diffraction information described in Fig. 8.

Fig. 8. The optical diffraction results from Fig. 7. Two of the precipitates, with smaller lattice parameter, are clearly identified. The third is not distinguished since its diffraction pattern is shared with that of the matrix.

Fig. 9. Schematic representation of the characteristics of spinodal decomposition plotted as concentration against distance (1) early stage (2) later stage.

Fig. 10. Series of optical microdiffractograms (~120Å equivalent dia.) from the lattice image of Fig. 7. (a) Cu-rich matrix, corresponding to position D in Fig. 7. (b) Cu-poor precipitate, corresponding to position A in Fig. 7. (c) Sharp interface, corresponding to position K in Fig. 7. (d) Diffuse interface, corresponding to position G in Fig. 7. (e) Modulated interface, corresponding to position C in Fig. 7.

Fig. 11. Schematic representation of a square-wave modulation with periodicity of 26 fringes (a). When each point is averaged over 15 fringes, a smooth waveform is produced. The introduction of statistical error (c) would make it very similar to the experimental plot of Fig. 5.

Table I. Fringe Spacing Measurements

(A) 700°C

Aging Time	Region	Direct Measurement from Micrograph	Microdensitometer	Optical Diffraction
10 min.	Cu-Rich	3.60 ± 0.10Å	3.60 ± 0.05Å	3.60 ± 0.02Å
	Cu-Poor	3.56 ± 0.10Å	3.56 ± 0.05Å	3.56 ± 0.02Å
166 hours	Cu-Rich	3.60 ± 0.10Å	3.61 ± 0.05Å	3.60 ± 0.02Å
	Cu-Poor	3.55 ± 0.10Å	3.56 ± 0.05Å	3.55 ± 0.02Å

(B) 600°C

Aging Time	Region	Direct Measurement from Micrograph	Microdensitometer	Optical Diffraction
1 hour	Cu-Rich	3.60 ± 0.10Å	3.60 ± 0.05Å	3.59 ± 0.02Å
	Cu-Poor	3.56 ± 0.10Å	3.57 ± 0.05Å	3.57 ± 0.02Å
808 hours	Cu-Rich	3.61 ± 0.10Å	3.61 ± 0.05Å	3.60 ± 0.02Å
	Cu-Poor	3.56 ± 0.10Å	3.55 ± 0.05Å	3.55 ± 0.02Å

0 0 0 0 4 7 0 8 5 9 0

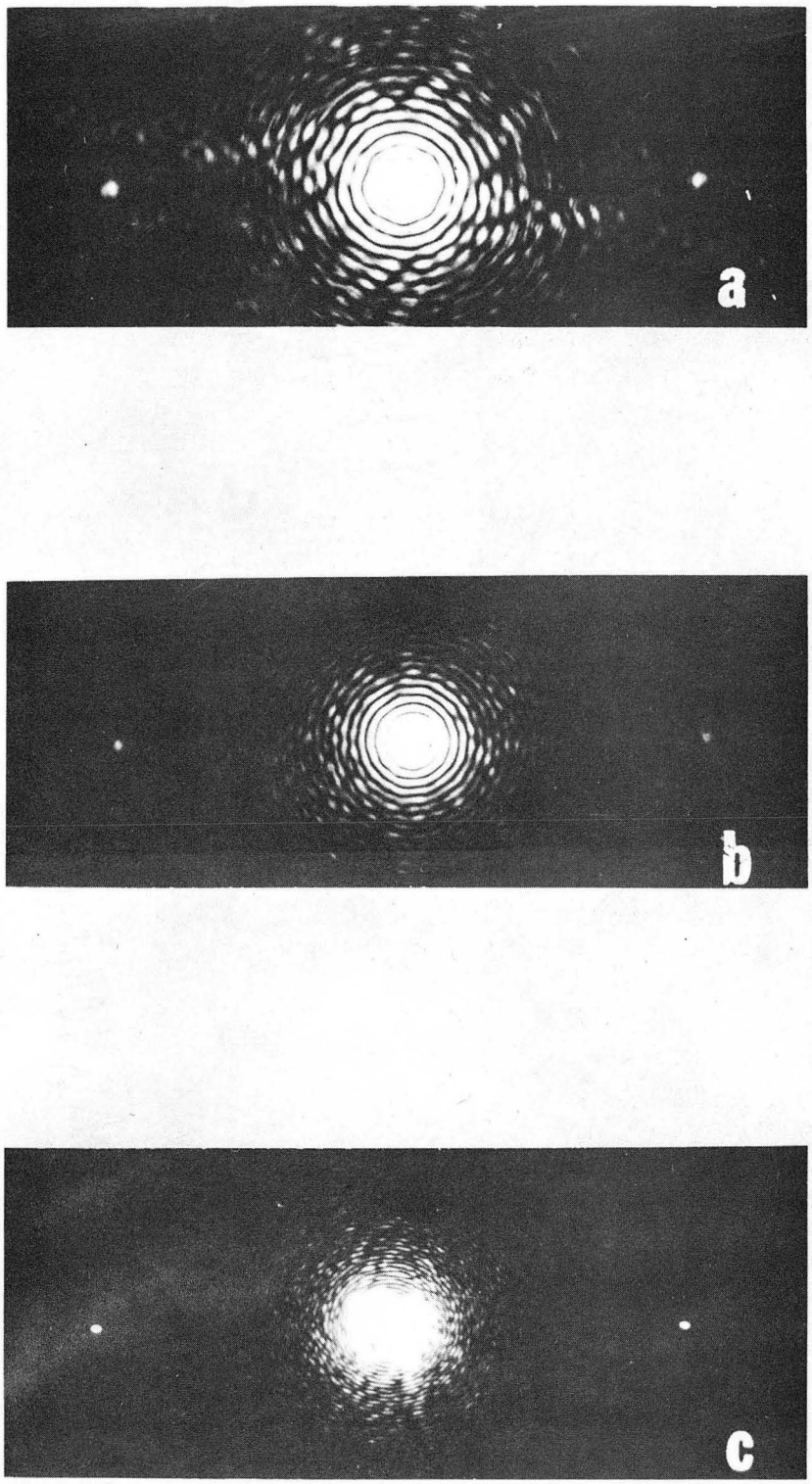

Fig. 1

XBB760-10144

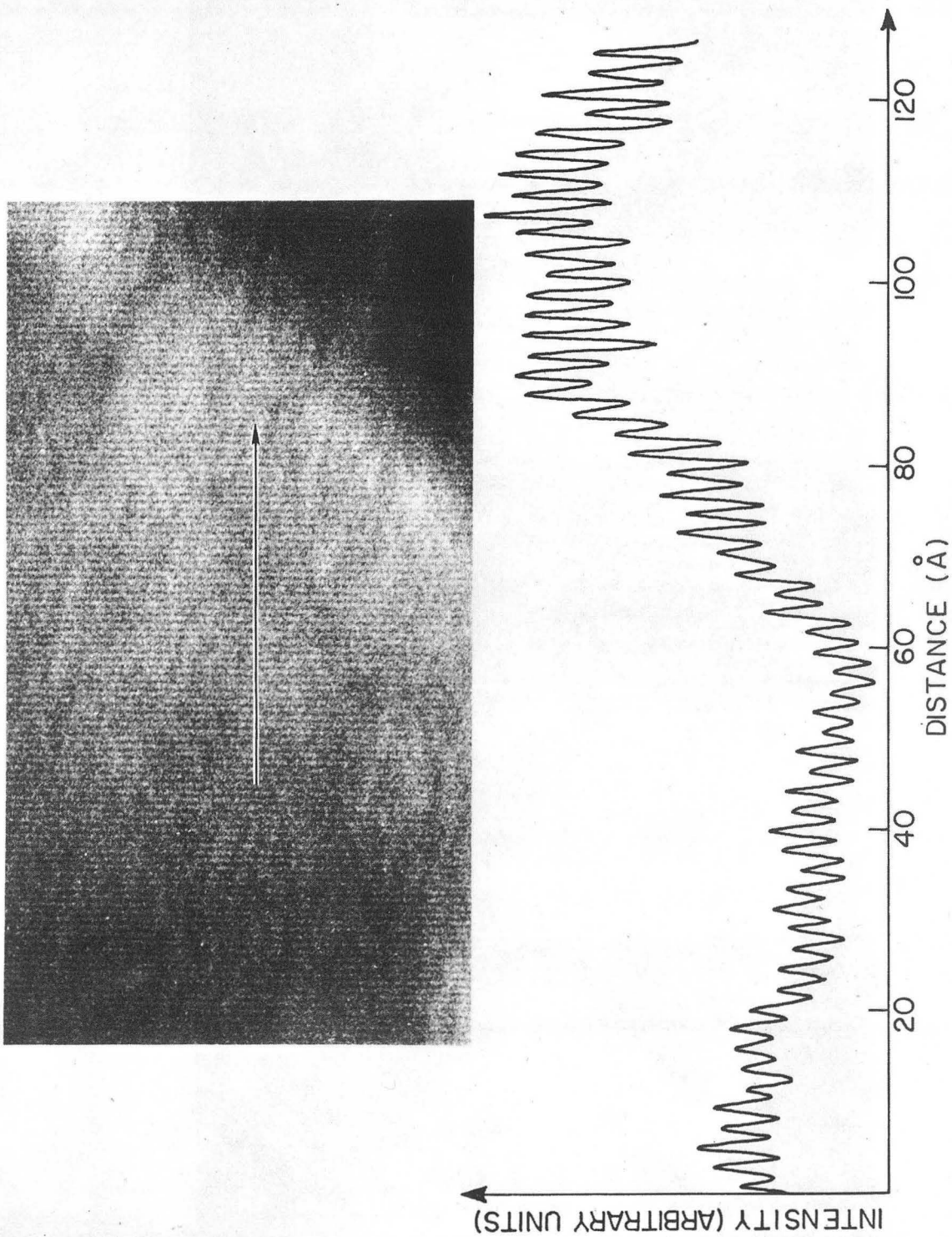

XBB760-11003

Fig. 2

0 0 0 0 4 7 0 8 5 9 1

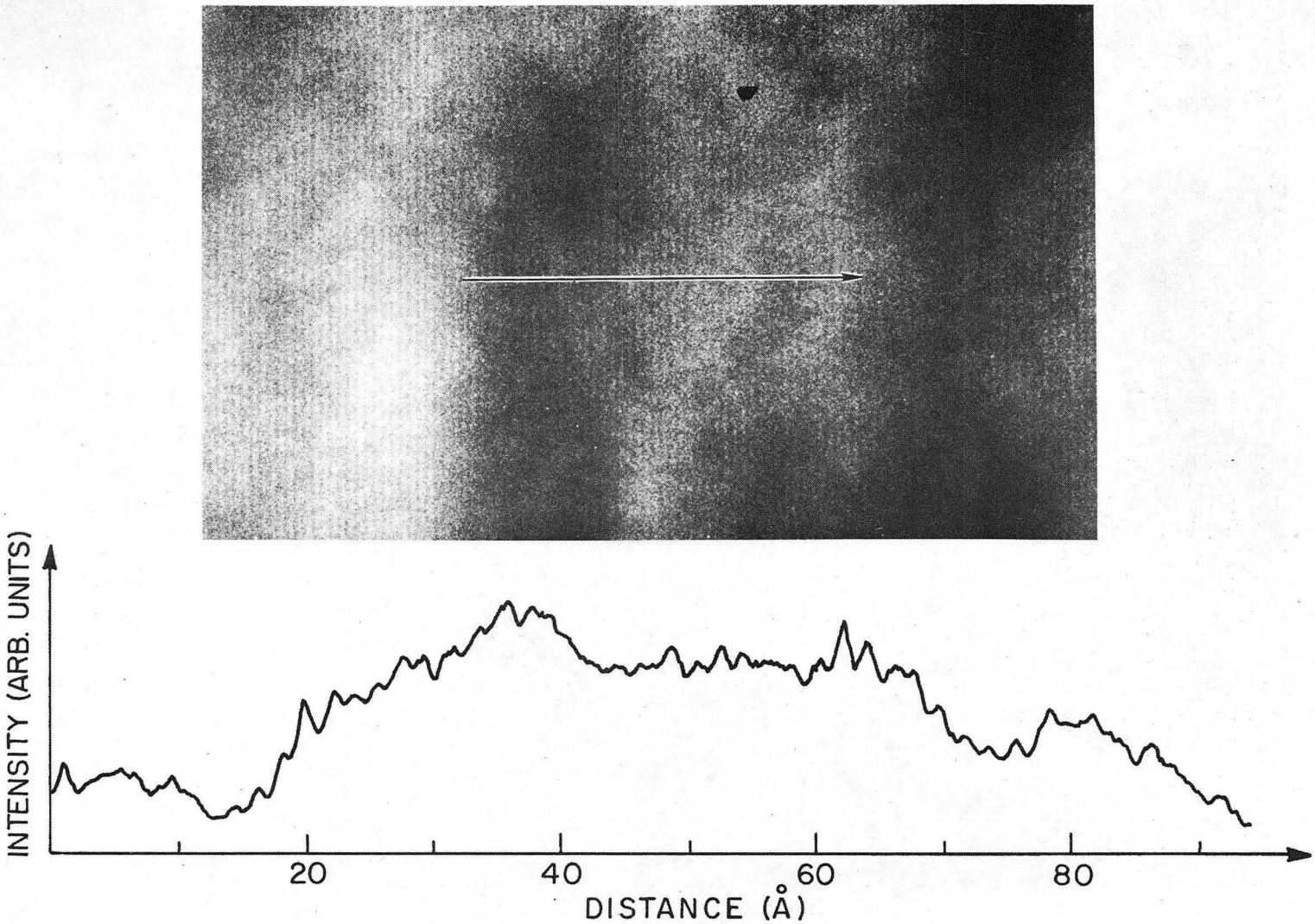

Fig. 3

XBB760-11002

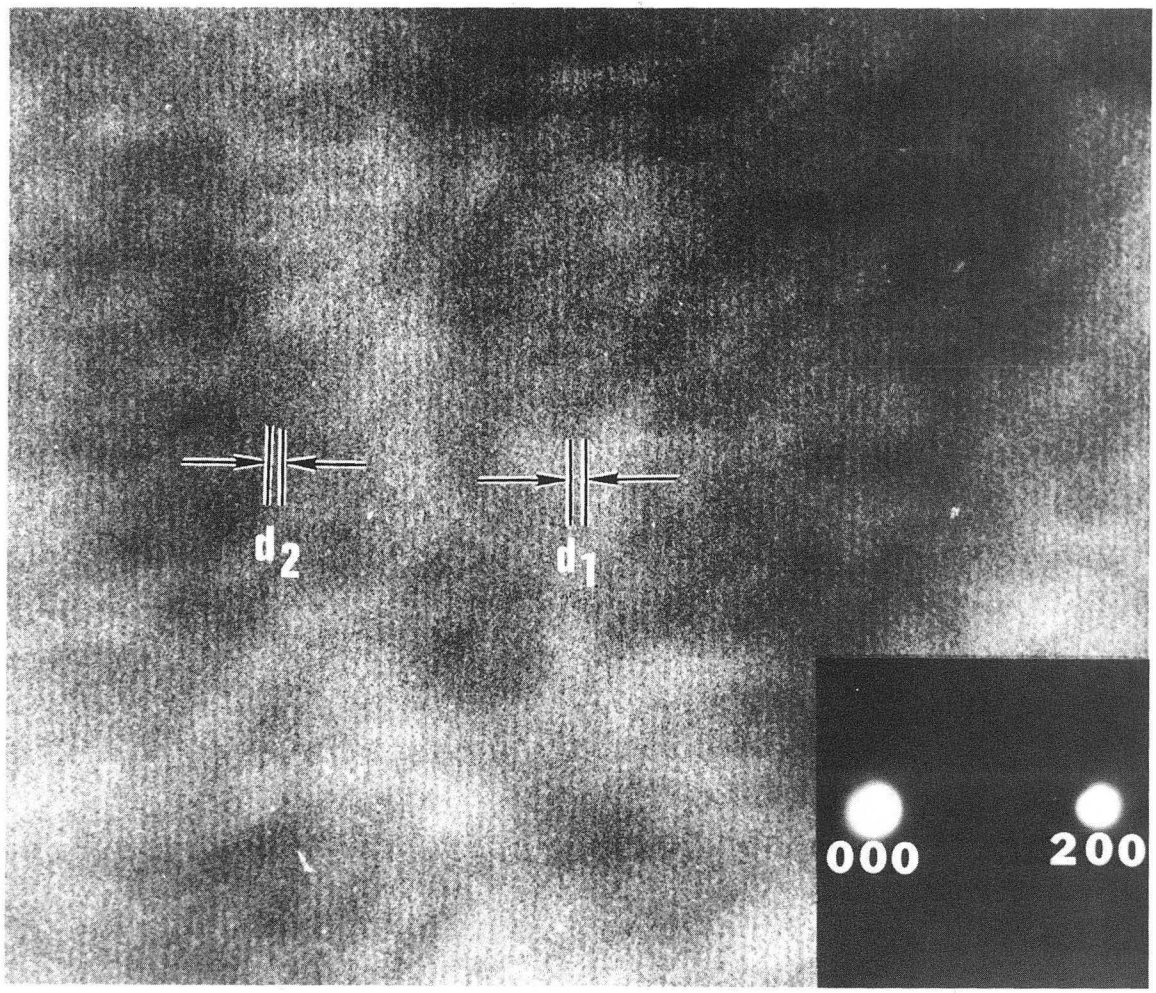

Fig. 4

XBB760-10136

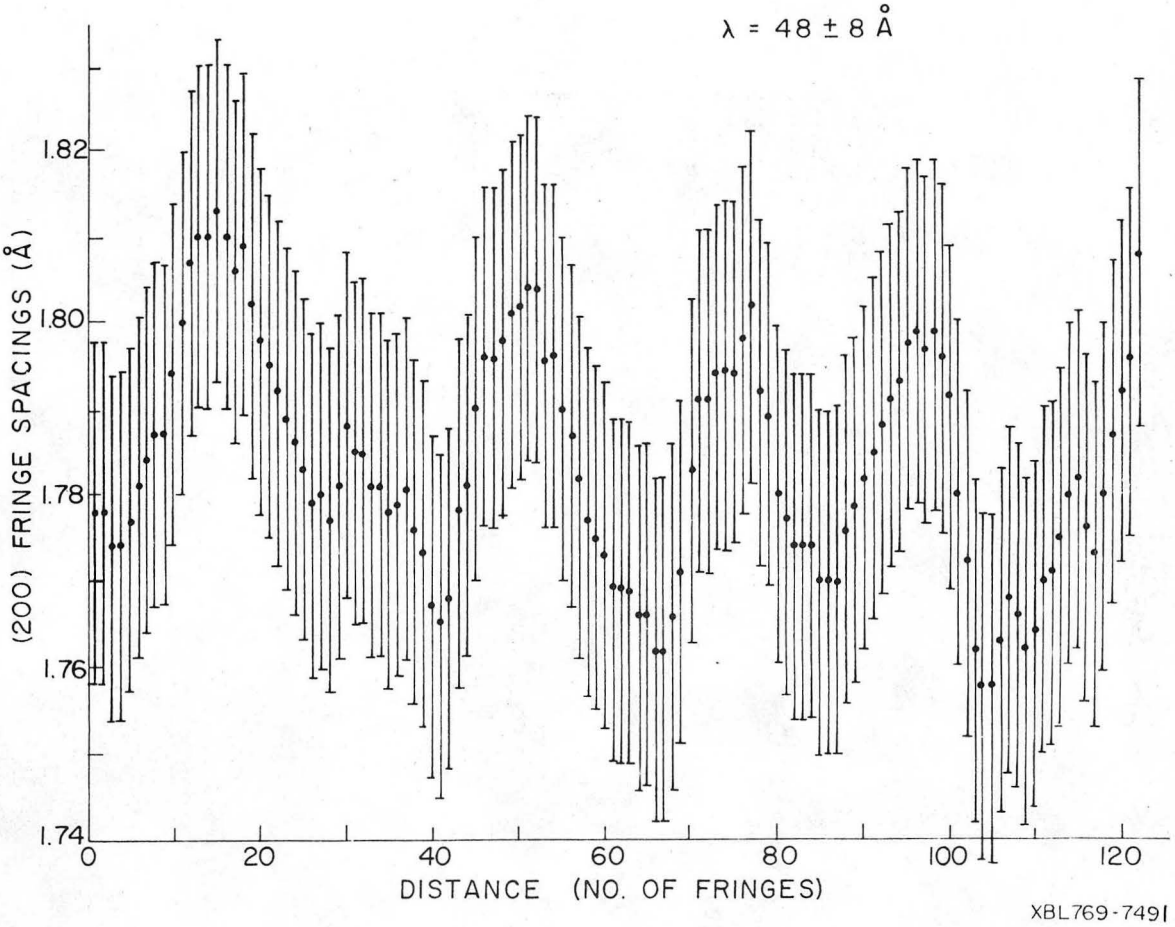
λ = 48 ± 8 Å
(200) FRINGE SPACINGS (Å)
1.82
1.80
1.78
1.76
1.74
0
20
40
60
80
100
120
DISTANCE (NO. OF FRINGES)
XBL769-7491

Fig. 5

Fig. 6

XBB772-1440

0 0 0 0 4 7 0 8 5 9 3

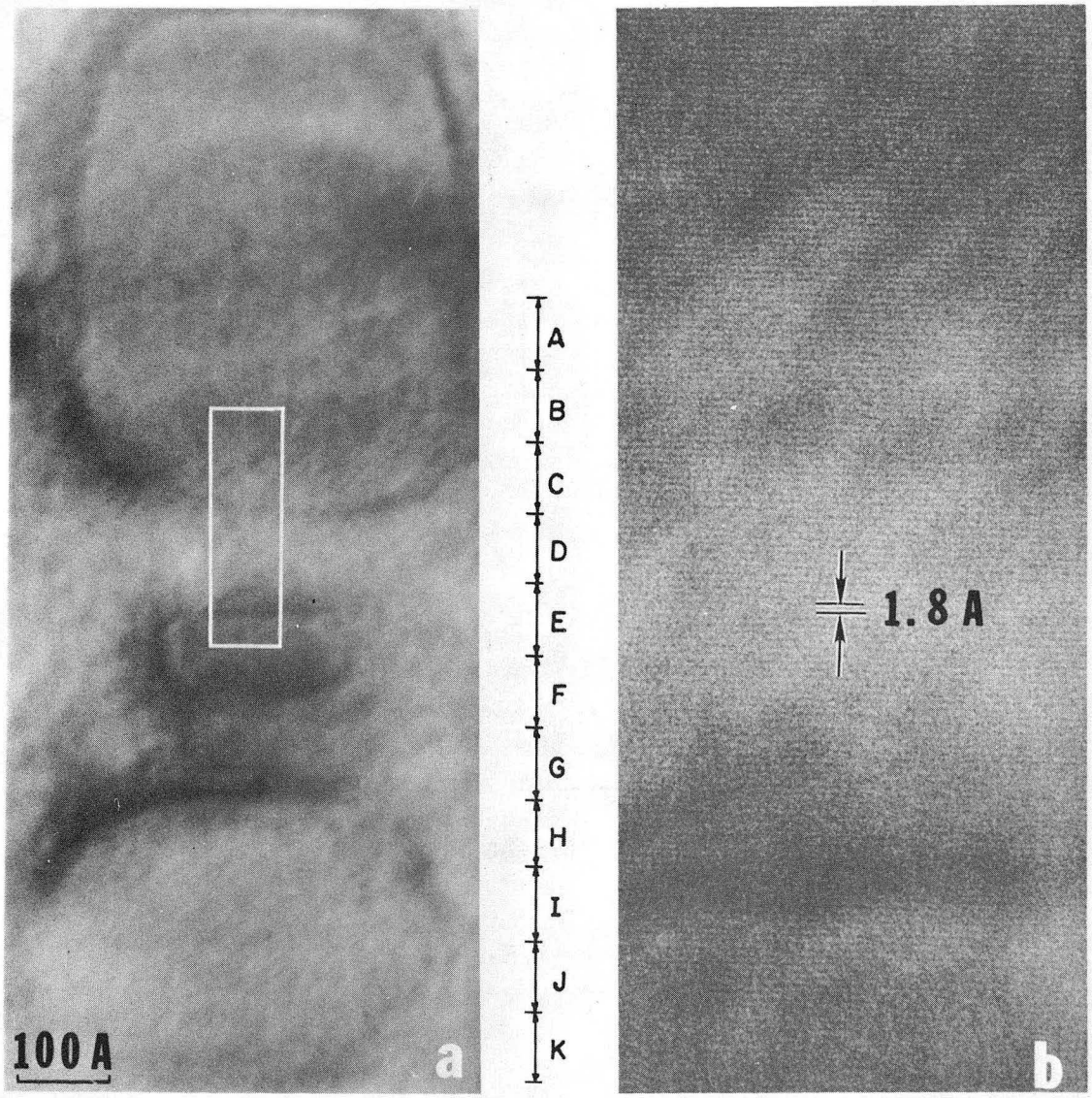

Fig. 7

XBB 778-7575

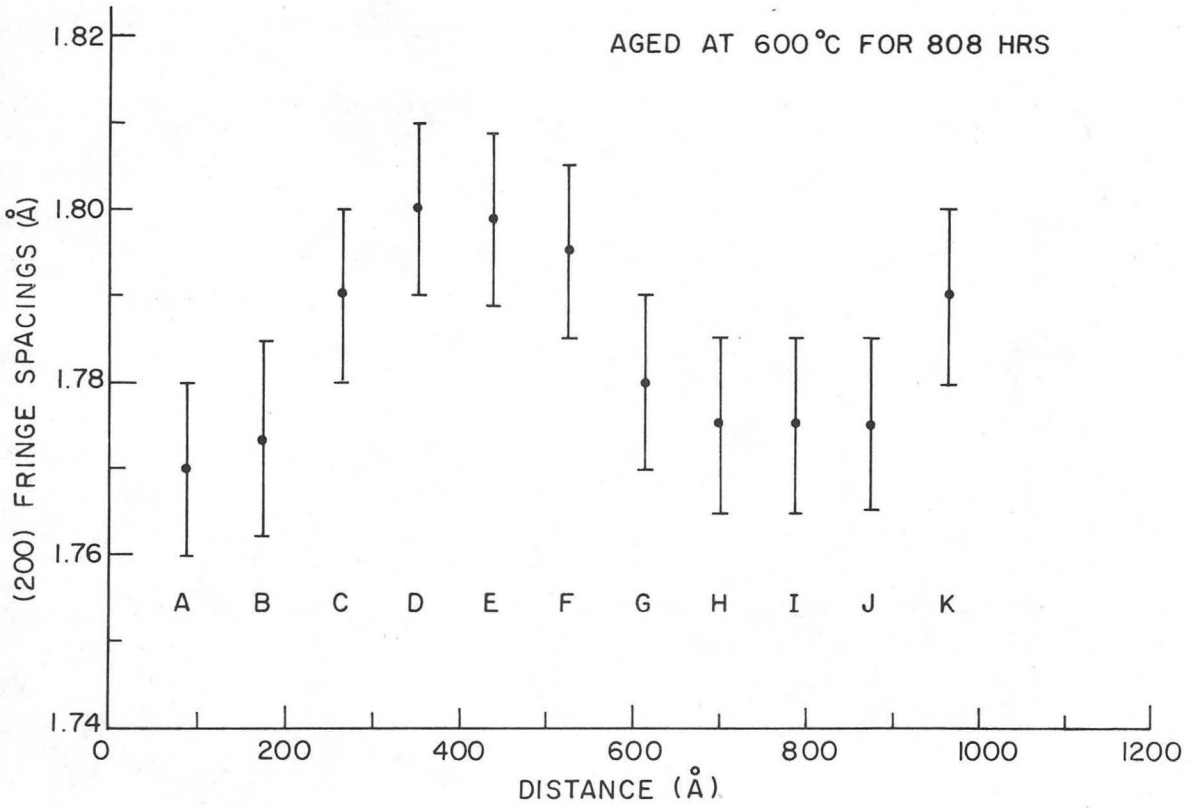

XBL 769-7497

Fig. 8

0 0 0 0 4 7 0 8 5 9 4

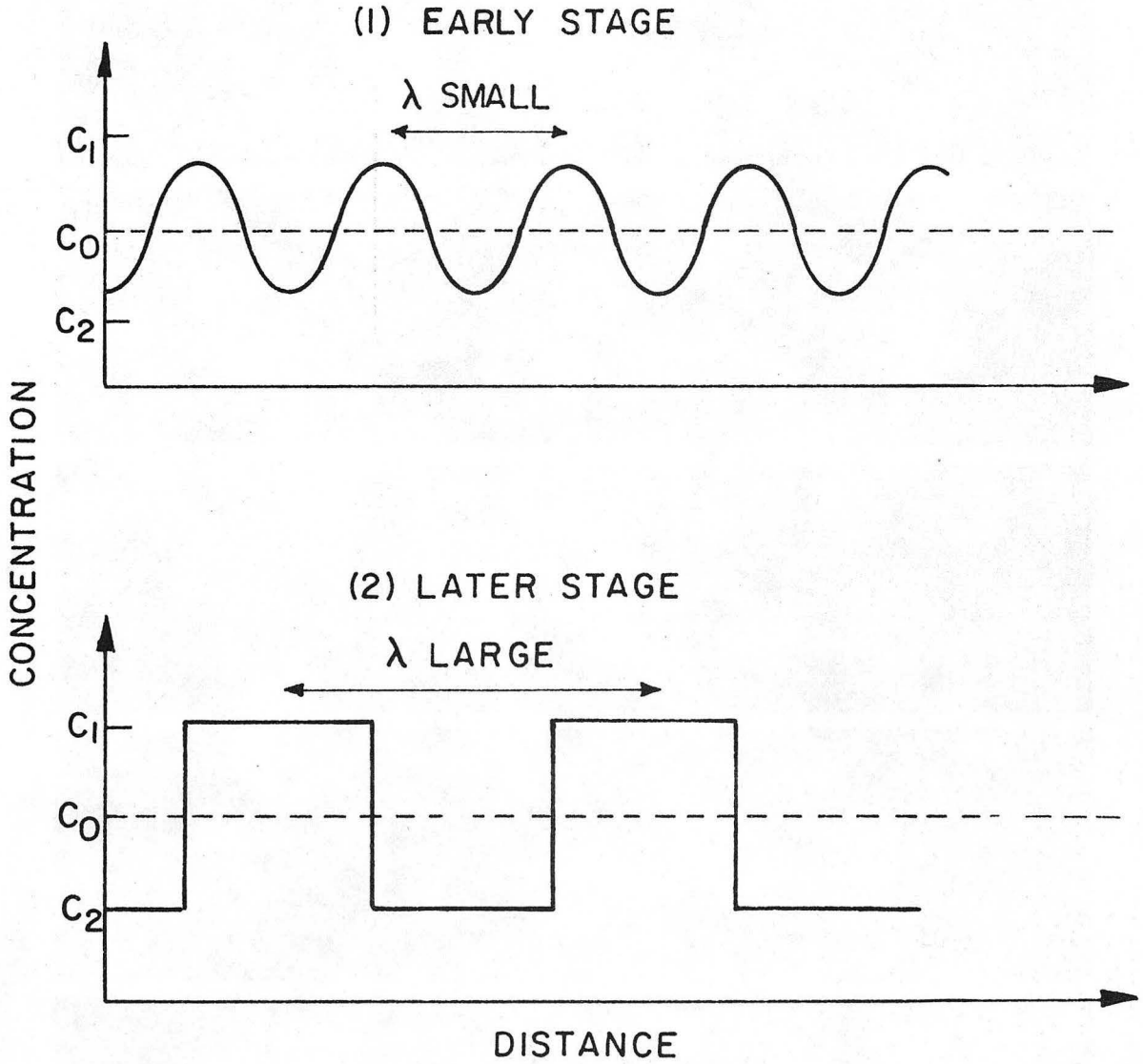

XBL 772-5042

Fig. 9

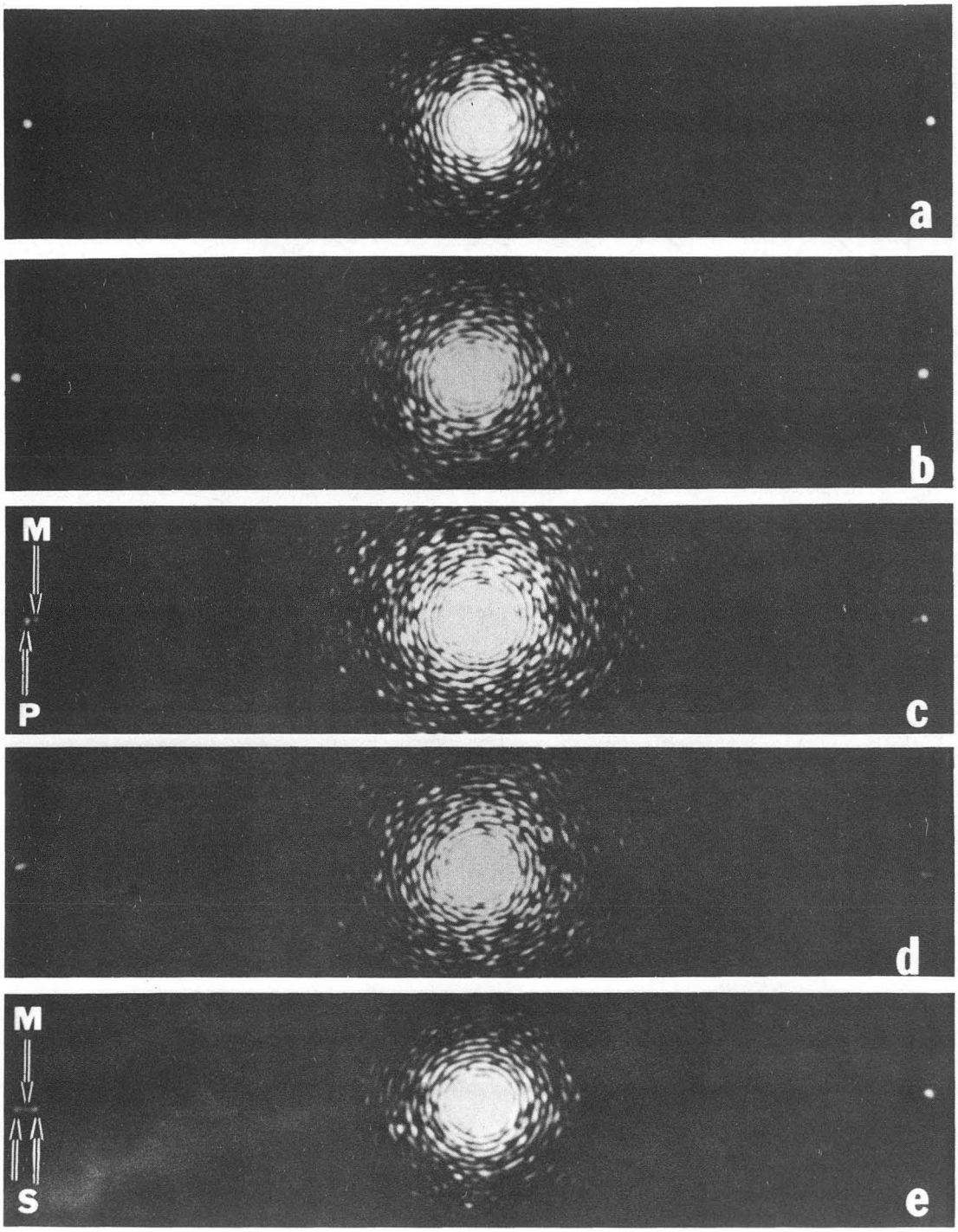

Fig. 10

XBB 778-7576

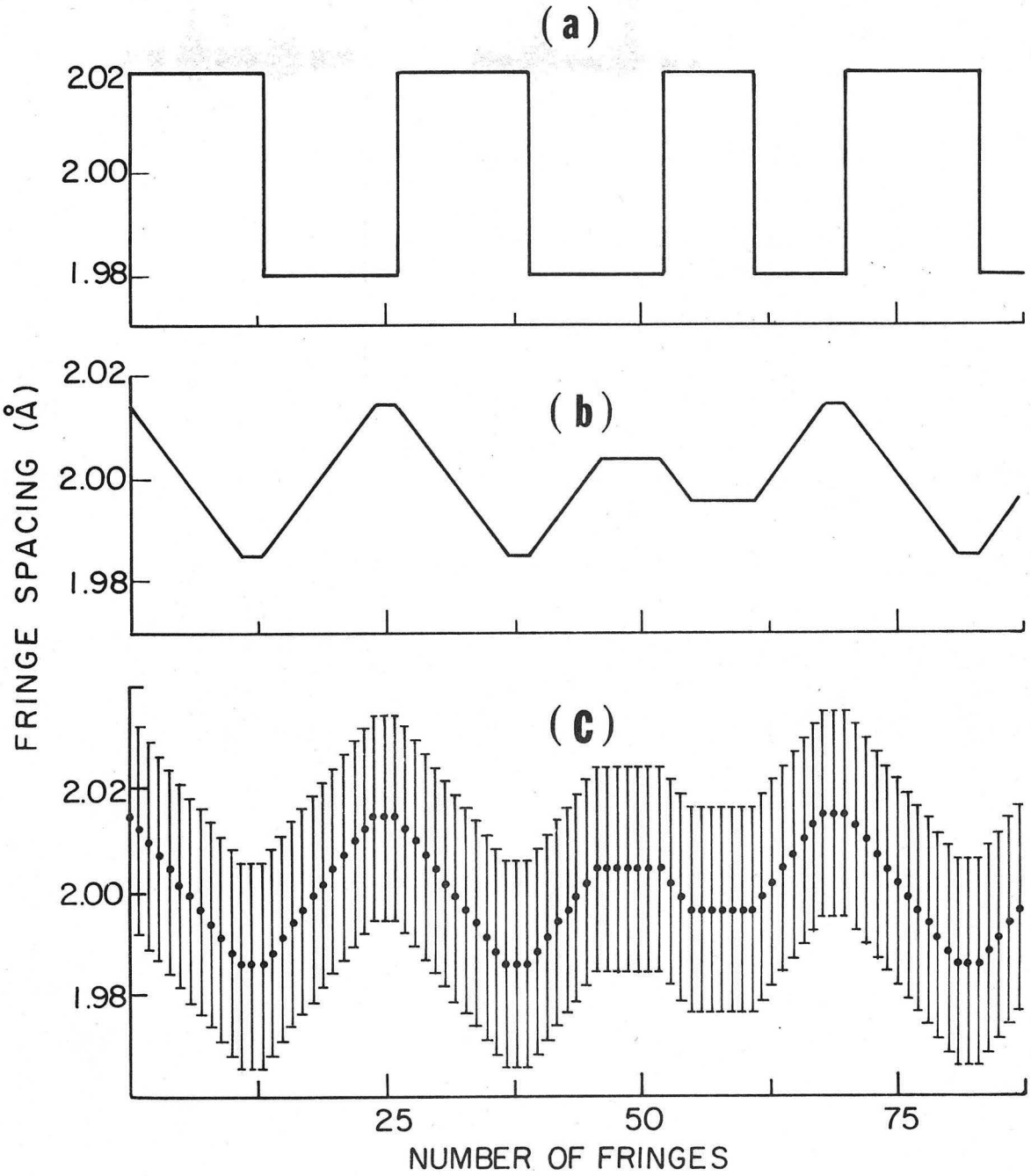

XBL774-5288

Fig. 11

0 0 0 0 4 7 0 0 3 9 5

This report was done with support from the Department of Energy. Any conclusions or opinions expressed in this report represent solely those of the author(s) and not necessarily those of The Regents of the University of California, the Lawrence Berkeley Laboratory or the Department of Energy.

TECHNICAL INFORMATION DEPARTMENT
LAWRENCE BERKELEY LABORATORY
UNIVERSITY OF CALIFORNIA
BERKELEY, CALIFORNIA 94720